2006

Analysis on Anti-Rotating Mechanism of New Symmetrical Wobble Plate Compressor

Zair Asrar Ahmad
Technical University of Malaysia

Ainullotfi Abdul Latif
Technical University of Malaysia

Ardiyansyah Syahrom
Technical University of Malaysia

Md. Nor Musa
Technical University of Malaysia

Analysis on Anti-Rotating Mechanism of New Symmetrical Wobble-plate Compressor

Zair Asrar AHMAD[1], Ainullotfi ABDUL-LATIF[2], Ardiyansyah SYAHROM[3], Md Nor MUSA[4]

[1]Faculty of Mechanical Engineering, Universiti Teknologi Malaysia
81300 Skudai, Johor, Malaysia
Tel: +607-5534878, Fax: +607-5566159, Email: zayax@yahoo.com

[2]Faculty of Mechanical Engineering, Universiti Teknologi Malaysia
Email: lotfi@fkm.utm.my

[3]Faculty of Mechanical Engineering, Universiti Teknologi Malaysia
Email: mr_ardy@yahoo.com.my

[4]Faculty of Mechanical Engineering, Universiti Teknologi Malaysia
Email: mdnor@fkm.utm.my

ABSTRACT

Axial piston compressors may be catagorised into two main types: wobble-plate and swash-plate compressors. Wobble-plate compressors differ from swash-plate ones by the use of an anti-rotation mechanism. This mechanism prevents the connecting rods from being tangled together by the wobble-plate from rotating with the rotor. Even though this mechanism enables the wobble-plate compressor to function correctly, it has also setbacks. From a new kinematics model of the wobble-plate mechanism proposed, the effects of the anti-rotation mechanism and related design parameters on the compressor motion were established. The actual loading characteristics on the anti-rotation mechanism were obtained, and then finite element analyses were done to check the structural integrity. Effects of other aspects of this new compressor design on the anti-rotation mechanism were also discussed.

1. INTRODUCTION

Amongst the many types of anti-rotation mechanisms used include bevel gear mechanisms, ball and anti-rotation rod mechanisms, Rzeppa mechanisms, and rod-with-sliding-plate mechanisms. Of all these mechanisms, the ball and anti-rotation is the most popular, easy to manufacture and reliable. As such, this mechanism was adopted in this new symmetrical multi-stage wobble-plate compressor design. The new design has two compression sides that resemble single-side fixed-capacity wobble-plate compressors that are joined together back-to-back. This design utilizes five-stage compression, thus requiring five piston sizes. The pistons were arranged axially around the shaft at angular intervals of 72°, starting from piston angular position, $\theta_i = 0°$.

2. KINEMATICS ANALYSIS

The wobble-plate motion can be obtained by understanding the motion of the connecting rod (Ishii *et. al*, 1990). The connecting rod ball-joint at the piston will show the piston motion while the connecting rod ball-joint at the wobble-plate will show the wobble-plate motion. Equations of motion for the pistons, connecting rods and wobble-plate are derived using standard coordinate transformation method.

2.1 Relationship between wobble-plate tilting angle and shaft rotation angle

The rotation of the inclined rotor, which is fixed to the shaft, will induce the wobble-plate wobbling motion. This motion can be expressed in term of the varying wobble-plate tilting angle, α, β and γ seen on the y-z, z-x and x_γ-z_γ planes respectively. The maximum wobble-plate tilting angle is the same as the rotor inclination angle or tilting

angle, $\tilde{\alpha}$, which moves as the shaft rotates. The relationship between the shaft angle of rotation, θ and α is given as $\alpha = \tilde{\alpha}\cos\theta$.

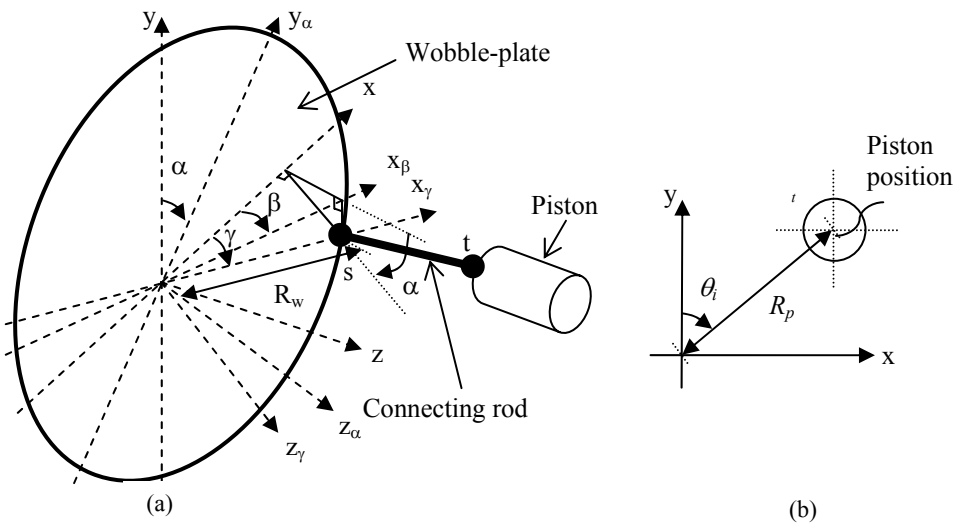

Figure 1: Location of the connecting rod ball: (a) on the wobble-plate side, (b) on the piston side

2.2 Motion of connecting rod ball-joint at wobble-plate side

From Fig. 1(a), the z-axis is taken to be coincident with the shaft axis while the y- and the x-axes are as shown. A guide-rod ball is placed at angular position θ_i = 180° on the wobble-plate periphery. At the guide rod location, wobble-plate movement is restricted to the in-plane motion in y-z plane. Using coordinate transformation, the movement of the connecting rod ball-joint on the wobble-plate side, *s* for i^{th} piston can be written as;

$$\left.\begin{aligned} x_s &= (R_w \sin\theta_i)\cos\gamma - (t_w)\sin\gamma \\ y_s &= (R_w \cos\theta_i)\cos\alpha - ((t_w)\cos\gamma + (R_w \sin\theta_i)\sin\gamma)\sin\alpha \\ z_s &= ((t_w)\cos\gamma + (R_w \sin\theta_i)\sin\gamma)\cos\alpha + (R_w \cos\theta_i)\sin\alpha \end{aligned}\right\} \quad (1)$$

β lags behind α by 90° and is given as $\beta = \tilde{\alpha}\sin\theta$. Angle γ is given by $\gamma = \tan^{-1}\left[\dfrac{\tan\beta}{\cos\alpha}\right]$

2.3 Motion of connecting rod ball-joint at piston side

From Fig. 1(b), the coordinate of the connecting rod ball on the piston side, *t*, is represented by:

$$\left.\begin{aligned} x_t &= R_p \sin\theta_i \\ y_t &= R_p \cos\theta_i \\ z_t &= ((t_w)\cos\gamma + (R_w \sin\theta_i)\sin\gamma)\cos\alpha + (R_w \cos\theta_i)\sin\alpha + l_{cr}\cos\phi_i \end{aligned}\right\} \quad (2)$$

With ϕ_i, as the angle between the connecting rod and the piston's axis is given as;

$$\phi_i = \sin^{-1}\left[\left\{(x_s - x_t)^2 + (y_s - y_t)^2\right\}^{1/2} / l_{cr}\right] \quad (3)$$

The value of x_t and y_t in equation (2) are constant for each θ_i. Only the position of the ball-joint at the piston side in z-axis, z_t, changes as shaft rotates.

2.4 Summary

By solving equation (1) for every piston position angle, θ_i, the locus of motion for point *s* for each piston is given in Fig. 2. This agrees with the locus of motion presented by Tojo *et al* (1988). The locus of motion is symmetrical in x_s and y_s axes. Locus of motion for the piston at angular position $\theta_i = 0°$ is the same as the locus of motion for the anti-rotation ball which has no motion in x_s axis. Considering the symmetrical locus of motion, the maximum number of anti-rotation mechanisms to be used is two. If θ_{ar} is chosen as the angular position of the anti-rotation rod, another possible angular position for the anti-rotation rod would be at (θ_{ar} +180°). Normally t_w = 0; thus α, β and γ are

maximum and minimum during maximum and minimum stroke. The magnitude of the maximum and the minimum angles between the connecting rod and piston axis from equation (3) are also the same. Maximum stroke occurs at $\theta = \theta_i$ while minimum stroke occurs at $\theta = (\theta_i+180°)$. Thus, the piston stroke, l, can be written as;

$$l = \left[R_w \sin\theta_i \sin\left(\tan^{-1}\left(\frac{\tan(\tilde{\alpha}\sin\theta)}{\cos(\tilde{\alpha}\cos\theta)} \right) \right) \cos(\tilde{\alpha}\cos\theta) + R_w \cos\theta_i \sin(\tilde{\alpha}\cos\theta) \right]$$
$$- \left[R_w \sin(\theta_i + 180°) \sin\left(\tan^{-1}\left(\frac{\tan(\tilde{\alpha}\sin\theta)}{\cos(\tilde{\alpha}\cos\theta)} \right) \right) \cos(\tilde{\alpha}\cos\theta) + R_w \cos(\theta_i + 180°) \sin(\tilde{\alpha}\cos\theta) \right] \quad (4)$$

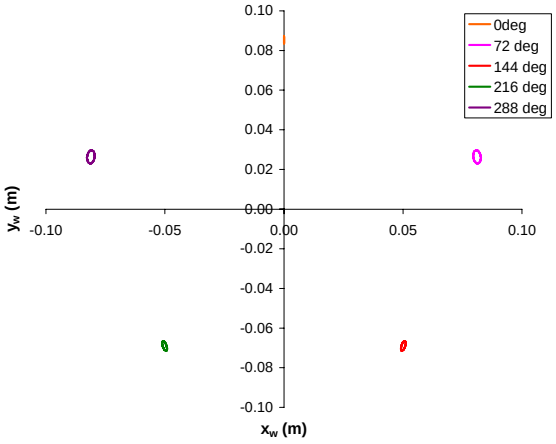

Figure 2: Locus of motion on the wobble-plate for each piston angular position

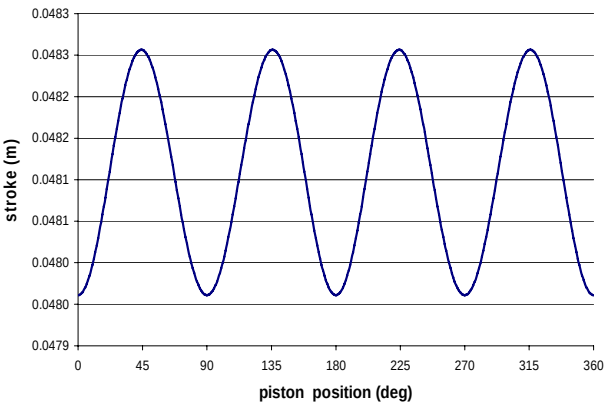

Figure 3: Stroke at various piston angular positions

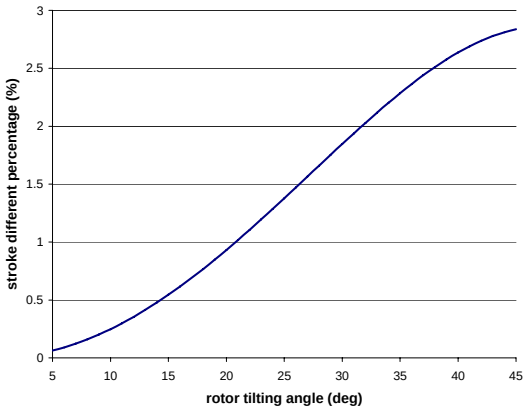

Figure 4: Effect of wobble-plate tilting angle, $\tilde{\alpha}$ on stroke difference percentage

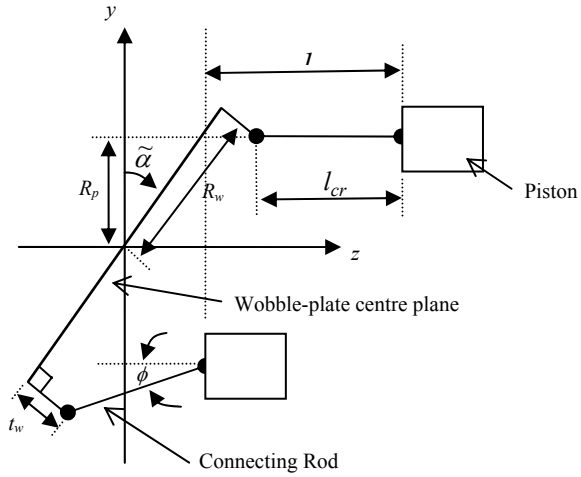

Figure 5: Piston stroke at angular piston position, $\theta_i = 0^\circ$

By calculating the piston stroke for all possible piston angular positions from $\theta_i = 0°$ to $\theta_i = 360°$ at 1° intervals; the piston stroke differs at each possible piston angular position as shown in Fig. 3. The piston stroke value is symmetrical in the x-axis and y-axis with the maximum value at θ_i equal to 45°, 135°, 225° and 315° and minimum at θ_i equal to 0°, 90°, 180° and 270°. By plotting for the variation of maximum wobble-plate tilting angle $\tilde{\alpha}$ from 5° to 45° as in Fig. 4; it is shown that the maximum stroke difference is less than three percent for value of $\tilde{\alpha}$ from 5° to 45°. Thus, the small stroke difference at each piston position can be omitted to ease the analysis procedure. The compressor piston stroke length is then taken to be at position $\theta_i = 0°$ as:

$$l = 2R_w \sin\tilde{\alpha} + l_{cr}(1-\cos\phi); \qquad \text{with } \phi = \tan^{-1}\left[\frac{2t_w \sin\tilde{\alpha}}{l_{cr}}\right] \tag{5}$$

Angular piston position $\theta_i = 0°$ is chosen because the wobble-plate motion at this angular position is in the *y-z* plane only as opposed to other points on the wobble-plate which involve more complex general motion as given in equation (1). The centre of the connecting rod ball-joint on the wobble-plate side will be placed at a normal distance t_w from the wobble-plate centre plane at shown in Fig. 5 and normally taken as zero in most of the existing wobble-plate compressor design. This is to reduce the maximum rotational degree of freedom needed at the ball-joint to $2\tilde{\alpha}$ rather than $2(\tilde{\alpha}+\phi)$ if t_w is not zero. A smaller rotational degree of freedom needed at the ball-joint means larger surface area available for retaining lip of the ball-joint. With $t_w = 0$, stroke equation is reduced to;

$$l = 2R_w \sin\tilde{\alpha} \tag{6}$$

The maximum ϕ_i for this new compressor design is around 2.5°. This gives $\sin\phi_i \approx 0$ and $\cos\phi_i \approx 1$. Thus variation of ϕ_i can also be omitted in the analysis, assuming that the connecting rod is always parallel to the shaft, to simplify the analysis. There are two suitable values for R_p, i.e. $R_p = R_w$ or $R_p = R_w\cos\tilde{\alpha}$. Both choices of R_p will give almost the same maximum value of ϕ_i. R_p should be chosen to be $R_p = R_w\cos\tilde{\alpha}$ to ensure connecting rod will be inline with piston during maximum stroke at TDC to reduce the side force from connecting rod to piston. However, as the difference between both choices of R_p on ϕ_i is small, R_p was chosen as $R_p = R_w$ to ease the designing process. The maximum piston velocity and acceleration for this new compressor design is about 3.8ms^{-1} and 600ms^{-2} respectively. The velocity and acceleration at each piston angular position also vary due to the difference in stroke length as shown in Fig. 6 and Fig. 7.

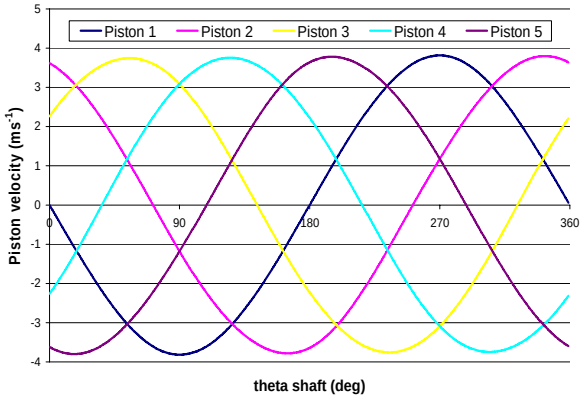

Figure 6: Variation of piston velocity at each stage

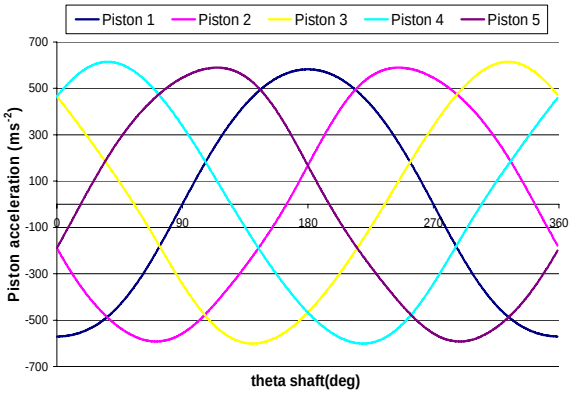

Figure 7: Variation of piston acceleration at each stage

3. LOADING ANALYSIS

Only one side of the compressor is needed in the analysis model due to the symmetrical configuration. The other side will have an effect on shaft loading and considered only in the shaft loading analysis whereby loading from right and left rotors will be included. The load on the pistons and the connecting rods are derived from the gas pressure load in global *x-y-z* axis coordinate. The summation of the loads from all connecting rods will act on the wobble-plate. To take the advantage of zero moment due to the bearing connection, loading analysis on the wobble-plate and rotor is done in the wobble-plate plane which is in *x'-y'-z'*. Thus, the moment about *z'*-axis is zero. The loads obtained from the rotors are then converted back to global axes values for shaft loading analysis. Loads and moments involved are transformed from global *x-y-z* axis to wobble-plate plane *x'-y'-z'* axis by pre-multiplying with transformation matrix $T_{g\text{-}p}$ as follows:

$$T_{g-p} = \begin{bmatrix} \cos(\theta) & -\sin(\theta) & 0 \\ \cos(\tilde{\alpha})\sin(\theta) & \cos(\tilde{\alpha})\cos(\theta) & \sin(\tilde{\alpha}) \\ -\sin(\tilde{\alpha})\sin(\theta) & -\sin(\tilde{\alpha})\cos(\theta) & \cos(\tilde{\alpha}) \end{bmatrix} \tag{7}$$

These forces and moments can be transformed back to global axes by pre-multiplying with transformation matrix $T_{p\text{-}g}$ which is equal to the inverse of $T_{g\text{-}p}$. Both matrices are obtained by knowing that the *x-y-z* axis is transformed to the *x'-y'-z'* axis by rotating it by $\tilde{\alpha}$ about the *x*-axis and θ about the *z*-axis and vice versa.

3.1 Loading on connecting rods

From the calculated piston position, the cylinder chamber volume at each shaft rotation instance was obtained. Gas pressure was then calculated through the compression process analysis using ideal compression cycle. The magnitude of the connecting rod force was obtained as

$$F_{crt_i} = \frac{A_{p_i} P_{gas_i} - M_{p_i} \ddot{z}_{t_i}}{\cos(\phi_i) - sign(\dot{z}_{t_i}) \cdot \mu_p \cdot \sin(\phi_i)} \tag{8}$$

3.2 Loading on wobble-plate

The translational and angular equations of motion for the wobble-plate are given in Fig. 8 and can be written as

$$\left.\begin{aligned} m_w \ddot{u}_w &= F_{wb} + F_{ar} + \sum_{i=1}^{i=ns} F_{crs} + W_w \\ M_{Iw} &= M_{ar} + \sum_{i=1}^{i=ns} M_{crs} + M_{wb} = (I_{wx}\ddot{\alpha})\hat{i} + (I_{wy}\ddot{\beta})\hat{j} - ((I_{wx} - I_{wy})\dot{\alpha}\dot{\beta})\hat{k} \end{aligned}\right\} \tag{9}$$

These equations are then solved in *x'*, *y'* and *z'* axis.

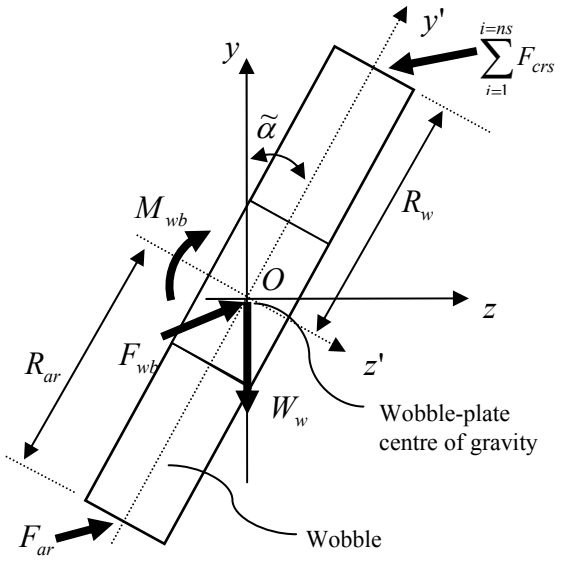

Figure 8: Loading on wobble-plate

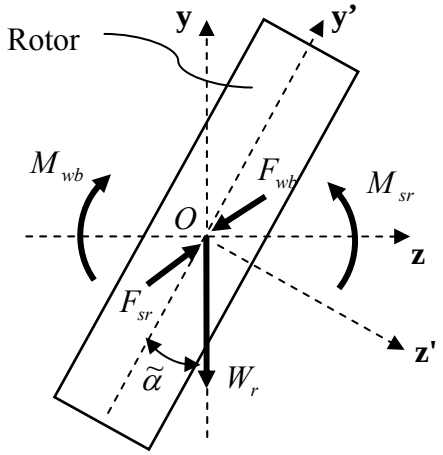

Figure 9: Loading on rotor

3.3 Loading on rotor

The translational and angular equations of motion for the rotor are given in Fig. 9 and can be written as

$$\left.\begin{aligned} m_r \ddot{u}_r &= F_{wb} + F_{sr} + W_r \\ M_{Ir} &= M_{sr} + M_{wb} \end{aligned}\right\} \tag{10}$$

The above equations are solved in *x'*, *y'* and *z'* axis. Due to the bearing interface between wobble-plate and rotor, moment transferred in *z'* axis is zero.

3.4 Loading on shaft

The calculated forces and moments on rotor are transferred back into global coordinate system in $x - y - z$ axis. From Fig. 10, Torque required to rotate shaft, *T*; can be obtained by solving for moment in z-axis as follows:

$$T = I_{sz}\ddot{\theta} - [M_{srz1} + M_{srz2}] = I_{sz}\ddot{\theta} - 2M_{srz} \tag{11}$$

At operating speed condition whereby $\ddot{\theta} = 0$, torque equation is reduced to $T = -2M_{srz}$. Due to symmetrical configuration, $F_{sr1} = F_{sr2} = F_{sr}$ and $F_{b1} = F_{b2} = F_b$. Thus, end plate bearing load can be obtained as

$$F_b = \frac{2F_{sr} + W}{2} \tag{12}$$

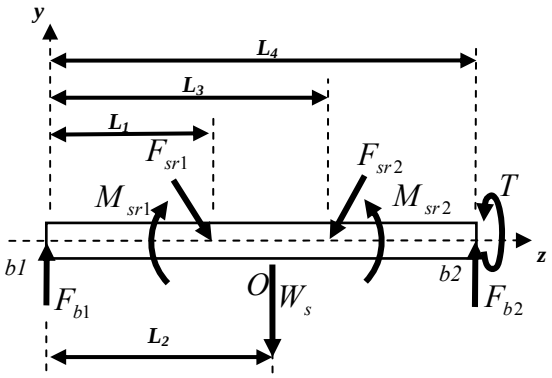

Figure 10: Loading on shaft

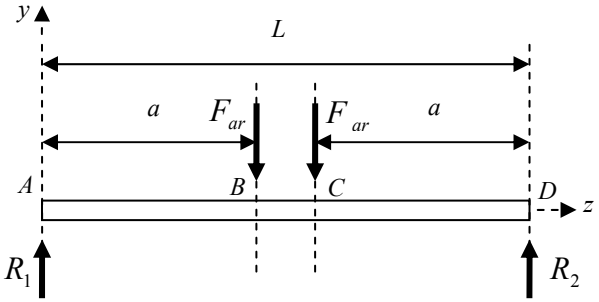

Figure 11: Loading on anti-rotation rod

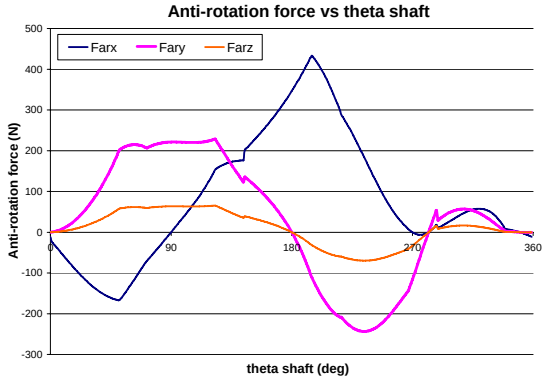

Figure 12: Component of force on the anti-rotation rod

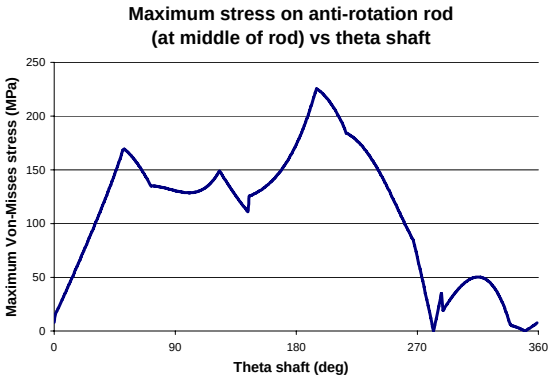

Figure 13: Stress on the anti-rotation rod

3.5 Loading on anti-rotation rod

The anti-rotation mechanism for this new compressor design consists of two balls which slide with both wobble-plates along the anti-rotation rod. Loading on anti-rotation rod is simplified as a beam with simple supports that has twin loads acting on it as in Fig. 11. The reactions at points *A* and *D* are obtained as $R_1 = R_2 = F_{ar}$. The moments at the spans *AB*, *BC* and *CD* are obtained as $M_{AB} = F_{ar}z$; $M_{BC} = F_{ar}a$; $M_{CD} = F_{ar}(L - z)$ respectively. The maximum beam deflection is at section *BC* and obtained as:

$$y_{\max} = \frac{F_{ar}a}{24EI}(4a^2 - 3L^2) \tag{13}$$

The corresponding maximum stress occuring in the anti-rotation rod is:

$$\sigma_{\max} = \frac{32F_{ar}a}{\pi D_{ar}^3} \tag{14}$$

The total length of the anti-rotation rod is the same as that of the shaft. Thus $L = L_4$ and $a = L_1 - z_{ar}$. The components of loads and maximum stress on the anti-rotation ball are given in Figures 12 and 13 respectively.

4. FINITE ELEMENT ANALYSIS

Finite element analysis was done using Abacus CAE to check the stress distribution and the deformation of the anti-rotation ball and the anti-rotation rod. Two sliding interactions exist which are between the wobble-plate slot surface and the anti-rotation ball surface, and between the anti-rotation ball surface and the anti-rotation rod surface. The former sliding interaction was modelled using contact interaction while the latter was tied together to reduce computational requirement. The anti-rotation rod was fixed at the surfaces supported by the left and the right end plates. Only the anti-rotation ball and the anti-rotation rod were modelled as deformable bodies. The wobble-plate was modelled as a rigid body consisting of the wobble-plate slot surface, the wobble-plate bearing surface and the loading points on the wobble-plate. These loading points are the centre of the connecting rod ball-joints at the wobble-plate. The wobble-plate bearing surface was coupled with the wobble-plate bearing centre of rotation point. The centre of rotation point was constrained to the ground using a revolute joint to simulate the bearing effect. The finite element analysis results are given in Table 1 and Table 2. Stress levels on the anti-rotation ball and anti-rotation rod are low and acceptable.

Table 1: Stress and displacement of anti-rotation rod

Stage of maximum pressure (piston at TDC)	Material yield strength (MPa)	Maximum von Mises stress (MPa)	Maximum anti-rotation rod displacement (m)	Safety factor
1 $(\theta = 0°)$	215	8.647	5.543×10^{-5}	24.88
2 $(\theta = 72°)$	215	30.87	1.611×10^{-4}	6.96
3 $(\theta = 144°)$	215	102.5	4.616×10^{-4}	2.10
4 $(\theta = 216°)$	215	93.49	4.459×10^{-4}	2.30
5 $(\theta = 288°)$	215	8.485	4.141×10^{-5}	25.34

Table 2: Stresses on anti-rotation ball

Stage of maximum pressure (piston at TDC)	Material yield strength (MPa)	Maximum Von-Mises stress (MPa)	Safety factor
1 $(\theta = 0°)$	215	2.467	87.15
2 $(\theta = 72°)$	215	19.78	10.87
3 $(\theta = 144°)$	215	27.66	7.77
4 $(\theta = 216°)$	215	33.01	6.51
5 $(\theta = 288°)$	215	3.048	70.54

5. PROTOTYPE TESTING

In this compressor design, oil-free lubrication method was used. Thus, the sliding of the anti-rotation ball surfaces need to be lubricated without using oil. In the first design, carbon was used as the material for the anti-rotation ball. Wear of the carbon ball created a film of carbon which lubricated the sliding surfaces. However with prolonged use, wear on the carbon anti-rotation ball created a gap between anti-rotation ball and wobble-plate slot. This gap caused knocking between the wobble-plate slot and the anti-rotation ball. Thus, after series of tests, the brittle carbon anti-rotation ball fractured due to this knocking impact. In the second design the anti-rotation ball material was then replaced with carbon filled PTFE that was much more durable. The same material was also used for the piston and the rider rings. Excessive shaft deflections caused the wobble-plate tilting angle to increase. As the tilting angle increased, stroke length increased accordingly, causing piston knocking in the cylinder liner. This knocking impact load was then transferred to the anti-rotation ball and anti-rotation rod. The knocking impact led to denting on one side of the anti-rotation ball. This deformation of the ball caused the anti-rotation rod to dent the shoe slot on the wobble-plate as it slides along the rod. To solve this problem, shaft deflection was reduced by introducing a support at the middle of shaft. A separate shoe is made as the sliding interface for the anti-rotation ball to prevent re-

fabrication of the whole wobble-plate component. Both anti-rotation ball and shoe material were also changed to tool steel. The sliding interface between these two components was then lubricated using metal sticking grease.

6. CONCLUSION

The maximum number of ball-and-rod anti-rotation mechanism to be used in a wobble-plate compressor design is two. Usage of this mechanism differentiates between the motion of a wobble-plate compressor and that of a swash-plate compressor. In the wobble-plate compressor, piston stroke, velocity and acceleration depend on the angular positions of the pistons whereas in the swash-plate compressor, all these parameters are constant at all piston angular positions. The anti-rotation mechanism structural integrity depends on the loading, the material and the lubrication method used. The behaviour of the anti-rotation mechanism can be used to indicate whether knocking has happened on piston or not as it will bend excessively and clearly to the human eye due to knocking impact force. Stress at five piston maximum compression positions as illustrated in Fig. 12 are higher than the results obtained using finite element analysis in Table 1. This is due to the beam idealisation in equations (13) and (14).

REFERENCES

Ishi, N., Abe, Y., Taguchi, T., Maruyama, T. and Kitamura, T., 1990, Dynamic Behaviour of Variable Displacement Wobble-plate Compressor for Automotive Air Conditioners, *Proc. Int. Compressor Conf.*, Purdue University, United States. pp. 345-353.

Tojo, K., Takao, K., Nakamura, Y., Kawasima, K. and Takahashi, Y., 1988, A Study on the Kinematics of a Variable Displacement Compressor for Automotive Air Conditioner. *Proc. Int. Compressor Conf.*, Purdue University, United States. pp. 496-504.

Ahmad, Z.A., Syahrom, A., Abdul-Latif, A. and Musa, M.N., 2003, Study on the Stressing of the New Symmetrical Wobble-plate Compressor: Kinematics and Forces. *Malaysia Science and Technology Congress*, Kuala Lumpur.

ACKNOWLEDGEMENT

The authors would like to thank the Ministry of Science, Technology and Innovation (MOSTI), Malaysia, and Universiti Teknologi Malaysia for providing the funding and the facilities to carry out this research.